



A novel method to calculate the magnetic field of a solenoid generated by a surface current element

Mostafa Behtouei^a, Bruno Spataro^a, Luigi Faillace^a, Martina Carillo^b,
Moreno Comelli ^c, Luigi Palumbo^{b,d}, Alessandro Variola^a and Mauro Migliorati^{b,d}

^aINFN, Laboratori Nazionali di Frascati, Frascati, Italy; ^bDipartimento di Scienze di Base e Applicate per l'Ingegneria (SBAI), Sapienza University of Rome, Rome, Italy; ^cInstitute of Applied Physics 'Nello Carrara', National Research Council, Sesto Fiorentino, Italy; ^dINFN/Roma1, Istituto Nazionale di Fisica Nucleare, Rome, Italy

ABSTRACT

The purpose of this paper is to derive the on and off-axes magnetic field of a solenoid with the use of a novel method. We have found a solution for the Biot-Savart law by considering the solenoid with a stationary electric current. The results have been compared to some simplified and known analytical formulae as well as to a numerical code showing a good agreement.

ARTICLE HISTORY

Received 16 December 2021
Accepted 8 August 2022

KEYWORDS

Particle acceleration; linear accelerators; accelerator applications; accelerator subsystems and technologies; mathematical physics

1. Introduction

The determination of the magnetic field of a solenoid is crucial in physics and engineering. For example, in linear accelerators such as high brilliance photoinjectors and in high gradient accelerating structures [1–6], in presence of the space charge, the effect of beam blow-up has to be thwarted with a solenoid. Moreover solenoid are used in magnetic correctors and steering devices for beam alignment [7].

We extend the results obtained in [8] by presenting the calculations to determine the magnetic field components of a solenoid with a finite length. Unlike the previous calculation [8], in this paper, we assume the solenoid is not formed by discrete coils but by a sheet of conductive material so that the current will be distributed on the surface of the solenoid, with a surface current density \mathbf{K} and comparing the results both with the numerical and the analytical results close to the axis of a circular coil.

2. Derivation of magnetic induction generated by a surface current element

Referring to Figure 1, and using cylindrical coordinates, the point \mathbf{p} where we want to determine the magnetic field has coordinates (r, γ, z) , while the position \mathbf{p}' of the infinitesimal element of the solenoid having surface current density \mathbf{K} is given by (R, α, z_0) . The vectors \mathbf{s}' and \mathbf{s} give the positions of the two points. With this notation, the Biot-Savart law for a

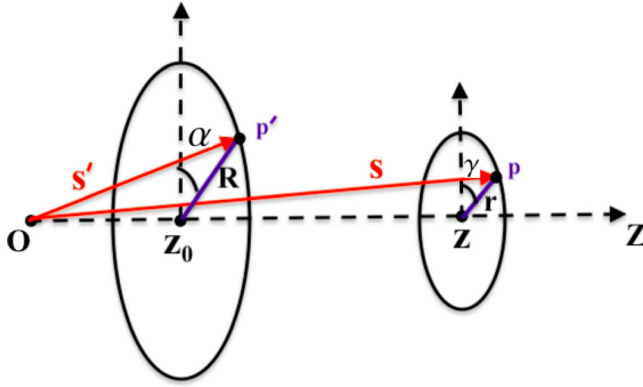


Figure 1. Off-axis field due to a volume current element. B is the magnetic field at any point in space out of the current loop. B_z is the magnetic field component in the direction of the coil axis. B_r is the radial magnetic field component. I is the current in the wire. R is the radius of the current loop. z is the distance, on axis, from the center of the current loop to the field measurement point. r is the radial distance from the axis of the current loop to the field measurement point α denotes for the angle of the current element γ stands for the angle of the observer where the magnetic field components are to be calculated.

solenoid of finite length can be written as,

$$\mathbf{B}(\mathbf{s}) = \frac{\mu_0}{4\pi} \int_{\Sigma} \frac{\mathbf{K} \times (\mathbf{s} - \mathbf{s}')}{|\mathbf{s} - \mathbf{s}'|^3} d\Sigma \quad (1)$$

where $\mathbf{K} d\Sigma$ is a surface current element in the direction of current flow. The surface current density \mathbf{K} and the infinitesimal surface element of solenoid $d\Sigma$ in cylindrical coordinates can be obtained:

$$\mathbf{K} = \frac{I}{\ell} \hat{\tau}, \quad d\Sigma = R d\alpha dz_0 \quad (2)$$

where ℓ is the length of the solenoid, $d\alpha$ is the infinitesimal variation of the angle and $\hat{\tau}$ stands for the unit vector tangent to the circumference of radius R and $d\alpha$, $\tau = -\hat{i} \sin \alpha + \hat{j} \cos \alpha$ with \hat{i} and \hat{j} the unit vectors along x and y , then Equation (1) becomes

$$\mathbf{B}(\mathbf{s}) = \frac{\mu_0 K}{4\pi} \int_{\Sigma} \frac{\hat{\tau} \times (\mathbf{s} - \mathbf{s}')}{|\mathbf{s} - \mathbf{s}'|^3} R d\alpha dz_0 \quad (3)$$

where cross product of $\hat{\tau}$ and $(\mathbf{p} - \mathbf{p}')$ is:

$$\begin{aligned} \hat{\tau} \times (\mathbf{s} - \mathbf{s}') &= \begin{vmatrix} \hat{i} & \hat{j} & \hat{k} \\ -\sin \alpha & \cos \alpha & 0 \\ r \cos \gamma - R \cos \alpha & r \sin \gamma - R \sin \alpha & z - z_0 \end{vmatrix} \\ &= \hat{i}(z - z_0) \cos \alpha + \hat{j}(z - z_0) \sin \alpha + \hat{k}(R - r \cos(\gamma - \alpha)) \end{aligned} \quad (4)$$

and

$$|\mathbf{s} - \mathbf{s}'|^2 = r^2 + R^2 + (z - z_0)^2 - 2rR \cos(\gamma - \alpha). \quad (5)$$

By some simplification Equation (1) becomes,

$$\begin{aligned} \mathbf{B}(\mathbf{s}) &= \frac{\mu_0 K}{4\pi} \int_0^{2\pi} \int_{-\ell/2}^{\ell/2} \frac{\hat{i}(z-z_0) \cos \alpha + \hat{j}(z-z_0) \sin \alpha + \hat{k}(R-r \cos(\gamma-\alpha))}{[r^2 + R^2 + (z-z_0)^2 - 2\rho R \cos(\gamma-\alpha)]^{3/2}} R d\alpha dz_0 \\ &= \frac{\mu_0 K}{4\pi} \int_0^{2\pi} \int_{-\ell/2}^{\ell/2} \frac{(\hat{i} \cos \alpha + \hat{j} \sin \alpha)(z-z_0) + \hat{k}(R-r \cos(\gamma-\alpha))}{[r^2 + R^2 + (z-z_0)^2 - 2rR \cos(\gamma-\alpha)]^{3/2}} R d\alpha dz_0. \end{aligned} \quad (6)$$

Writing the components of the magnetic field along the x, y and z coordinates, $\mathbf{B}(\mathbf{s}) = B_x \hat{i} + B_y \hat{j} + B_z \hat{k}$, and then converting them to the cylindrical coordinates we obtain

$$B_r = \mathbf{B}(\mathbf{s}) \cdot \mathbf{r} = B_x \cos \gamma + B_y \sin \gamma \quad (7)$$

$$B_\gamma = \mathbf{B}(\mathbf{s}) \cdot \hat{\tau} = -B_x \sin \gamma + B_y \cos \gamma \quad (8)$$

where,

$$\hat{\tau} = (-\sin \gamma, \cos \gamma, 0) \quad (9)$$

$$\mathbf{r} = (\cos \gamma, \sin \gamma, 0). \quad (10)$$

After some algebraic manipulation we obtain,

$$\begin{aligned} B_r &= \frac{\mu_0 K}{2\pi} \int_{-M_{z\ell}}^{M_{z\ell}} (M_z - M_{z_0}) [1 + \eta^2 + (M_z - M_{z_0})^2]^{-3/2} dM_{z_0} \\ &\quad \times \int_0^\pi \cos(\psi) [1 - \Lambda \cos(\psi)]^{-3/2} d\psi \end{aligned} \quad (11)$$

$$\begin{aligned} B_\gamma &= \frac{\mu_0 K}{2\pi} \int_{-M_{z\ell}}^{M_{z\ell}} (M_z - M_{z_0}) [1 + \eta^2 + (M_z - M_{z_0})^2]^{-3/2} dM_{z_0} \\ &\quad \times \int_0^\pi \sin(\psi) [1 - \Lambda \sin(\psi)]^{-3/2} d\psi \end{aligned} \quad (12)$$

$$\begin{aligned} B_z &= \frac{\mu_0 KR}{2\pi} \int_{-M_{z\ell}}^{M_{z\ell}} [1 + \eta^2 + (M_z - M_{z_0})^2]^{-3/2} dM_{z_0} \\ &\quad \times \left[\int_0^\pi [1 - \Lambda \cos(\psi)]^{-3/2} d\psi - \eta \int_0^\pi \cos(\psi) [1 - \Lambda \cos(\psi)]^{-3/2} d\psi \right] \end{aligned} \quad (13)$$

where $\eta = \rho/R$, $M_z = z/R$ and $\Lambda(R, z, \eta) = 2\eta/(1 + \eta^2 + M_z^2)$. To solve the above integrals we had to deal with two fractional integrals of order $3/2$. We solved these integrals by using fractional Cauchy-like integral formula. We cut the created branch line and change the multi-valued operation into the analytic function. The procedure can be found in [8],

$$\int_0^\pi [1 - \Lambda \cos(\psi)]^{-3/2} d\psi = \pi(1 + \Lambda)^{-3/2} {}_2F_1\left(\frac{1}{2}, \frac{3}{2}; 1; \frac{2\Lambda}{1 + \Lambda}\right) \quad (14)$$

$$\begin{aligned} \int_0^\pi \cos(\psi) [1 - \Lambda \cos(\psi)]^{-3/2} d\psi &= -\pi(1 + \Lambda)^{-3/2} \\ &\quad \left[{}_2F_1\left(\frac{1}{2}, \frac{3}{2}; 1; \frac{2\Lambda}{1 + \Lambda}\right) - {}_2F_1\left(\frac{3}{2}, \frac{3}{2}; 2; \frac{2\Lambda}{1 + \Lambda}\right) \right] \end{aligned} \quad (15)$$

where ${}_2F_1\left(\frac{1}{2}, \frac{3}{2}; 1; \frac{2\Lambda}{1+\Lambda}\right)$ and ${}_2F_1\left(\frac{1}{2}, \frac{3}{2}; 1; \frac{2\Lambda}{1+\Lambda}\right)$ are the ordinary hypergeometric functions having a general form of the kind

$${}_pF_q(a_1, \dots, a_p; b_1, \dots, b_q; z) = \sum_{n=0}^{\infty} \frac{(a_1)_n \dots (b_p)_n}{(b_1)_n \dots (b_p)_n} \frac{z^n}{n!} \tag{16}$$

where $(a_p)_n, (b_q)_n$ are the rising factorial or Pochhammer symbol with

$$(a)_0 = 1 \tag{17}$$

and

$$(a)_n = a(a+1)(a+2) \dots (a+n-1), \quad n = 1, 2, \dots \tag{18}$$

It should be noted that Equation (12) is zero due to azimuthal symmetry. By changing of variables Equations (11) and (13) become,

$$\begin{aligned} B_r &= \frac{\mu_0 K}{2} \int \frac{\sqrt{(1+\eta)^2 + (M_z + M_{z\ell})^2}}{\sqrt{(1+\eta)^2 + (M_z - M_{z\ell})^2}} \frac{1}{\beta^2} \left[{}_2F_1\left(\frac{1}{2}, \frac{3}{2}; 1; \frac{4\eta}{\beta^2}\right) - {}_2F_1\left(\frac{3}{2}, \frac{3}{2}; 2; \frac{4\eta}{\beta^2}\right) \right] d\beta \\ &= \frac{\mu_0 K}{2} \frac{1}{\beta} \left[{}_2\bar{F}_1\left(\frac{3}{2}, \frac{1}{2}; 2; \frac{4\eta}{\beta^2}\right) - {}_2\bar{F}_1\left(\frac{1}{2}, \frac{1}{2}; 1; \frac{4\eta}{\beta^2}\right) \right] \Bigg|_{\sqrt{(1+\eta)^2 + (M_z - M_{z\ell})^2}}^{\sqrt{(1+\eta)^2 + (M_z + M_{z\ell})^2}} \end{aligned} \tag{19}$$

and

$$\begin{aligned} B_z &= \frac{-\mu_0 K}{2} \int \frac{\sqrt{(1+\eta)^2 + (M_z + M_{z\ell})^2}}{\sqrt{(1+\eta)^2 + (M_z - M_{z\ell})^2}} \frac{1}{\beta^2 (\beta^2 - (1+\eta)^2)^{1/2}} \left[{}_2F_1\left(\frac{1}{2}, \frac{3}{2}; 1; \frac{4\eta}{\beta^2}\right) \right. \\ &\quad \left. + \eta \left({}_2F_1\left(\frac{1}{2}, \frac{3}{2}; 1; \frac{4\eta}{\beta^2}\right) - {}_2F_1\left(\frac{3}{2}, \frac{3}{2}; 2; \frac{4\eta}{\beta^2}\right) \right) \right] d\beta \end{aligned} \tag{20}$$

with,

$$\beta = [(1+\eta)^2 + (M_z - M_{z0})^2]^{1/2} \tag{21}$$

where ${}_2\bar{F}_1\left(\frac{3}{2}, \frac{1}{2}; 2; \frac{4\eta}{\beta^2}\right)$ and ${}_2\bar{F}_1\left(\frac{1}{2}, \frac{1}{2}; 1; \frac{4\eta}{\beta^2}\right)$ are the regularized hypergeometric functions having a general form of the kind

$${}_p\bar{F}_q(a_1, \dots, a_p; b_1, \dots, b_q; z) = \sum_{n=0}^{\infty} \frac{(a_1)_n \dots (b_p)_n}{\Gamma(b_1 + n) \dots \Gamma(b_p + n)} \frac{z^n}{n!} \tag{22}$$

where $(a_p)_n, (b_q)_n$ are the rising factorial or Pochhammer symbol with $(a)_0$ and $(a)_n$ are the same as Equations (17) and (18). We could also write the regularized hypergeometric functions in a simple way ${}_p\bar{F}_q(a_1, \dots, a_p; b_1, \dots, b_q; z) = (\Gamma(b_1) \dots \Gamma(b_p))^{-1} {}_pF_q(a_1, \dots, a_p; b_1, \dots, b_q; z)$. To validate Equations (19) and (20) we would investigate the on axis field components. We observe that the regularized hypergeometric functions in Equation (19) cancel each other and consequently the radial field component becomes zero. On the other hand, for on axis axial field components we can derive a classic equation which can be found in

many physics textbooks and papers [8–10]:

$$B_z = \frac{\mu_0 I R^2}{2(R^2 + z^2)^{3/2}}. \quad (23)$$

The near axis magnetic field components have been expressed by the authors of [10] as follows,

$$B_r(r, z) = 2 \sum_{p=0}^{\infty} p G_{S2p}(z) r^{2p-1} \quad (24)$$

$$B_z(r, z) = \sum_{p=0}^{\infty} G_{S2p+1}(z) r^{2p} \quad (25)$$

where,

$$G_{S2p}(z) = \frac{\mu_0 I_c}{2R^{2p} Z_L} \sum_{k=0}^{\infty} F_{0,2p,2k+1} [f_{2k+1}(Z_L - z) + f_{2k+1}(Z_L + z)] \quad (26)$$

$$G_{S2p+1}(z) = \frac{dG_{S2p}(z)}{dz} \quad \text{and} \quad g_{2k+1}(t) = \frac{df_{2k+1}}{dt} = \frac{(2k+1)R^2}{(R^2 + (Z-z)^2)^{3/2}} f_{2k}(t). \quad (27)$$

with the following definitions,

$$f_h(t) = \left(\frac{Z-z}{\sqrt{R^2 + (Z-z)^2}} \right)^h, \quad (h = 0, 1, \dots, \infty) \quad (28)$$

$$F_{0,2p,2k+1} = \frac{(-1)^p}{4^p (p!)^2} (M^p F_{00})_{2k+1} \quad (29)$$

where M stands for the second derivative of functions f_{2k+1} and F_{00} is reported in [10]. Taking the first two terms of the magnetic field components we obtain:

$$B_r(r, z) = \frac{\mu_0 J_S}{4} \left[\frac{3R^2(Z_L - z)}{(R^2 + (Z_L - z)^2)^{5/2}} - \frac{3R^2(Z_L + z)}{(R^2 + (Z_L + z)^2)^{5/2}} \right] r \quad (30)$$

$$B_z(r, z) = \frac{\mu_0 J_S R^2}{2} \left[\frac{R^2 + (Z_L - z)^2 - 3r^2}{(R^2 + (Z_L - z)^2)^{5/2}} - \frac{R^2 + (Z_L + z)^2 - 3r^2}{(R^2 + (Z_L + z)^2)^{5/2}} \right] \quad (31)$$

where the total current of the solenoid being I_S , the density function $J_S(Z)$ on its lateral surface is:

$$J_S(Z) = \frac{I_S}{2Z_L} [u(Z + Z_L) - u(Z - Z_L)]. \quad (32)$$

A solenoid is considered as a set of coils uniformly covering the space between $-Z_L$ and Z_L . Equation (30) is coincident with Equation (19) when we consider the first two terms in the regularized expansion of the hypergeometric series ${}_2\bar{F}_1\left(\frac{3}{2}, \frac{1}{2}; 2; \frac{4\eta}{\beta^2}\right)$ and ${}_2\bar{F}_1\left(\frac{1}{2}, \frac{1}{2}; 1; \frac{4\eta}{\beta^2}\right)$.

3. Numerical results

WebNIR [11] (Web-based tools for assessing occupational exposure to Non-Ionizing Radiation), a portal collecting a series of tools for dissemination and calculation developed as part of a collaboration with other research institutions on exposure to electromagnetic fields, has been developed at the Institute of Applied Physics ‘Nello Carrara’ of the National

Research Council (IFAC-CNR). One of these tools, still under development, allows the user to define different types of configurations of conductors (polygonal chains, catenaries, coils, solenoids), define both their geometric and electrical characteristics (current, phase, waveform) and calculate the value of magnetic flux density in correspondence to a set of regularly distributed points in the space (the calculation grid). Two different approaches have been used to perform the calculation: (1) since the field of a segment traversed by current is known, any geometry can be approximated by a polygonal chain consisting of an arbitrarily large number of segments; calculating the field generated by each of them, the resulting field is given by the sum of the individual contributions; (2) for a circular loop, the analytical solution of the field in the space is known [8, 12]: consequently, the field generated by geometries consisting of a set of circular loops (e.g.: coils, solenoids) is determined exactly by considering the elementary contribution of each loop. An 'internal validation' of the software results has been carried out by comparing the results obtained by applying, in the case of a solenoid:

- the formulation using the complete elliptic integrals of first and second kind [12]

$$B_r = \frac{\mu_0 I}{2\pi r \sqrt{z^2 + (a+r)^2}} \left(\frac{z^2 + r^2 + a^2}{z^2 + (r-a)^2} E(k) - K(k) \right) \quad (33)$$

$$B_z = \frac{\mu_0 I}{2\pi \sqrt{z^2 + (a+r)^2}} \left(\frac{a^2 - z^2 - r^2}{z^2 + (r-a)^2} E(k) + K(k) \right) \quad (34)$$

- the formulation that uses the hypergeometric function [8]

$$B_r = \frac{\mu_0 I M_z}{4\sqrt{2}\pi R} \left(\frac{\Lambda}{\eta} \right)^{3/2} I_2(\Lambda) \quad (35)$$

$$B_z = \frac{\mu_0 I}{4\sqrt{2}\pi R} \left(\frac{\Lambda}{\eta} \right)^{3/2} (I_1(\Lambda) - \eta I_2(\Lambda)) \quad (36)$$

where,

$$I_1(\Lambda) = \int_0^\pi [1 - \Lambda \cos(\psi)]^{-3/2} d\psi = \pi(1 + \Lambda)^{-3/2} {}_2F_1 \left(\frac{1}{2}, \frac{3}{2}; 1; \frac{2\Lambda}{1 + \Lambda} \right) \quad (37)$$

$$\begin{aligned} I_2(\Lambda) &= \int_0^\pi \cos(\psi) [1 - \Lambda \cos(\psi)]^{-3/2} d\psi \\ &= -\pi(1 + \Lambda)^{-3/2} \left[{}_2F_1 \left(\frac{1}{2}, \frac{3}{2}; 1; \frac{2\Lambda}{1 + \Lambda} \right) - {}_2F_1 \left(\frac{3}{2}, \frac{3}{2}; 2; \frac{2\Lambda}{1 + \Lambda} \right) \right]. \end{aligned} \quad (38)$$

We can demonstrate that the magnetic field components obtained by two different methods are identical following the below equations:

$$E \left(\frac{2\Lambda}{\Lambda + 1} \right) = \frac{\pi}{2} \frac{1 - \Lambda}{1 + \Lambda} {}_2F_1 \left(1/2, 3/2, 1, \frac{2\Lambda}{\Lambda + 1} \right) \quad (39)$$

$${}_2F_1 \left(3/2, 3/2, 2, \frac{2\Lambda}{\Lambda + 1} \right) = \frac{4E \left(\frac{2\Lambda}{\Lambda + 1} \right) + \left(\frac{\Lambda - 1}{\Lambda + 1} \right) K \left(\frac{2\Lambda}{\Lambda + 1} \right)}{\frac{2\pi\Lambda(1-\Lambda)}{(\Lambda+1)^2}} \quad (40)$$

where $K(k)$ and $E(k)$ are the complete elliptic integrals of the first and second kind, respectively.

- the approximate calculation in which the helix which constitutes the solenoid is approximated with a polygonal chain. The number of segments constituting the single loop has been progressively increased in different tests (in detail, the loop was approximated with 20, 200 and 2000 segments).

The result obtained in the first 2 cases is coincident up to the 13th digit: the 2 formulations are equivalent and the discrepancies are due to the approximations implicit in the libraries used. In particular, the language used to perform the calculations is Python 3.9 and the library `scipy.special` deals with calculating elliptic integrals and hypergeometric functions.

Comparison of these results with those obtained from the approximation with a polygonal chain showed a progressive convergence as the number of segments with which the helix is approximated increases.

Finally, in the center of a solenoid with the following characteristics: 200 loops, radius = 25 mm, distance between loops = 1 mm and current intensity = 200 A, the result coincides with that expected from the theoretical formula for the infinite solenoid, given by $B = \frac{\mu_0 NI}{\ell}$ where N indicates the number of loops, I the current, ℓ the length of the solenoid and μ_0 is the magnetic permeability in vacuum. With the specified parameters we obtain: $B = 8 \times 10^{-2} T \approx 0.25 T$ which is consistent with the numerical results obtained through the software in WebNIR, as shown in Figures 2–4. Figure 2 shows the numerical result of the B_z component along the axis of the solenoid ($\eta = r/R = 0$, $R = 25$ mm). The results are obtained through the use of the tool in WebNir. Figure 3(a,b) shows the trend of B_z and B_r for an off-axis case of 20 mm, respectively. The trend of B_z and B_r orthogonally to the solenoid

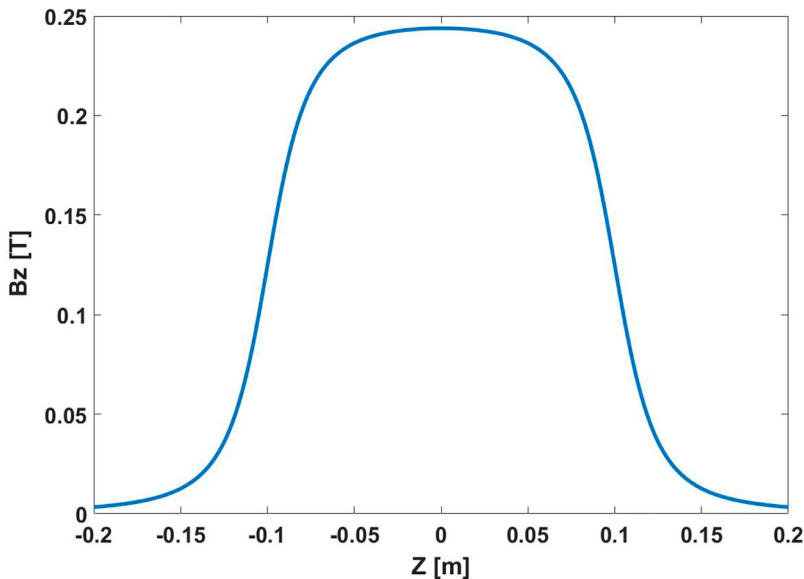


Figure 2. Trend of the B_z component along the axis of the solenoid (the radial component is zero), the results are obtained through the use of the tool in WebNir.

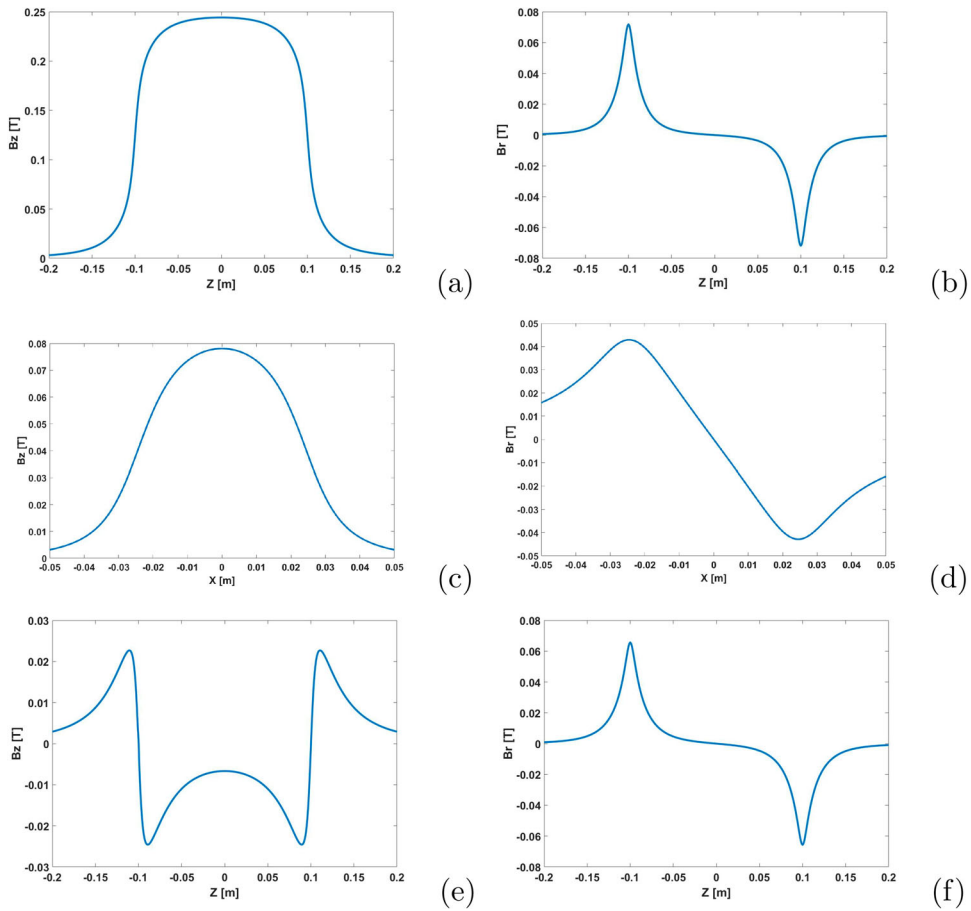


Figure 3. (a,b) Trend of B_z and B_r 2 cm off axis, (c,d) Trend of B_z and B_r orthogonally to the solenoid axis, 1 cm off the inlet, (e,f) Trend of B_z and B_r 0.5 cm off solenoid. The results are obtained through the use of the tool in WebNir.

axis with 10 mm off the inlet can be observed respectively in Figure 3(c,d). The field components of B_z and B_r with the 5 mm off solenoid are shown in Figure 3(e ,f), respectively. The results are obtained through the use of the tool in WebNir. Figure 4(a) and shows the modulus of B_z on a longitudinal section, through the center of the solenoid. The modulus of B_r on a longitudinal section is shown in Figure 4(b). The results are performed using the tool in WebNir.

4. Conclusions

The computation of the induction obtained theoretically was compared with a computation obtained independently, and both the mathematical equivalence of the two analytical derivations and the exact correspondence with the simple case of the field along the axis of the loop were demonstrated. Furthermore, the implementation within an independently developed software allowed once again to successfully compare the results obtained with the two methods (which use in the final formulation the complete elliptic integrals of the

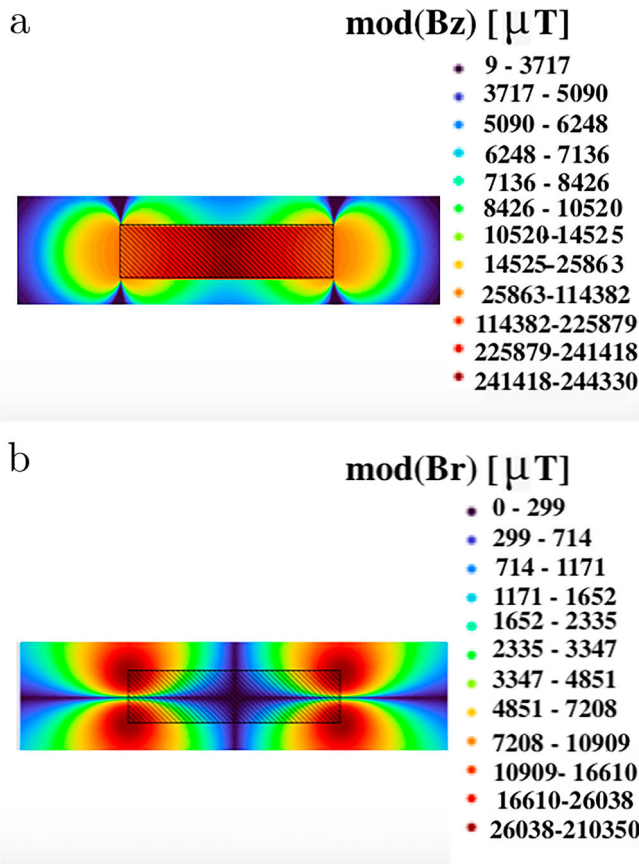


Figure 4. (a) Modulus of B_z on a longitudinal section, through the center of the solenoid. (b) Modulus of B_r on a longitudinal section, through the center of the solenoid. the results are obtained through the use of the tool in WebNir.

first and second species and the hypergeometric functions, respectively) and verify their consistency both with the simple case of the field along the axis, and with the approximate calculation for a solenoid of infinite length (analytically calculable).

Disclosure statement

No potential conflict of interest was reported by the author(s).

ORCID

Moreno Comelli  <http://orcid.org/0000-0001-9776-0943>

References

- [1] Ferrario M, Alesini D, Bacci A, et al. Direct measurement of the double emittance minimum in the beam dynamics of the SPARC high-brightness photoinjector. *Phys Rev Lett.* 2007;99(23):234801.
- [2] Migliorati M, Dattoli G. Transport matrix of a solenoid with linear fringe field. *Il Nuovo Cimento Soc Ital Fis-B.* 2009;124(4):385.

- [3] Stratakis D, Gallardo JC, Palmer RB. Effects of external magnetic fields on the operation of high-gradient accelerating structures. *Nucl Instrum Methods Phys Res A*. 2010;620(2–3):147–154.
- [4] Nezhevenko OA, et al. 34.3 GHz accelerating structure for high gradient tests, PACS2001. Proceedings of the 2001 Particle Accelerator Conference (Cat. No. 01CH37268). Vol. 5. IEEE; 2001.
- [5] Behtouei M, Faillace L, Ferrario M, et al. Initial design of a high-power Ka-band klystron. *J Phys: Conf Ser*. 2020;1596:012023.
- [6] Behtouei M, Spataro B, Di Paolo F, et al. The Ka-band high power klystron amplifier design program of INFN. *Vacuum*. 2021;191:110377.
- [7] Brady LW, Yaeger TE. *Encyclopedia of radiation oncology*; 2013.
- [8] Behtouei M, Faillace L, Spataro B, et al. A novel exact analytical expression for the magnetic field of a solenoid. *Waves Random Complex Media*. 2020.
- [9] Jackson JD. *Classical electrodynamics*. New York: John Wiley & Sons, Inc.; 1999.
- [10] Bassetti M, Biscari C. Analytical formulae for magnetic multipoles. *Part Accel*. 1996;52:221–250.
- [11] Web-based tools for assessing occupational exposure to Non-Ionizing Radiation. Institute of Applied Physics ‘Nello Carrara’ of the National Research Council (IFAC-CNR). Available from: <https://webnir.eu>
- [12] Grant Trebbin. Deriving the expression for the off-axis magnetic field of a circular current loop. Available from: <https://www.grant-trebbin.com/2012/04/off-axis-magnetic-field-of-circular.html>